

Interpretation of Gravity and Magnetic Anomalies over the
Southern Continental Shelf of Sri Lanka

by

Suraweera Arachchilage Dinesha Lakmal Kumara Suraweera



Thesis submitted to the University of Sri Jayewardenepura for the
award of the Degree of Master of Philosophy in Geophysics in
2013.

“The work described in this thesis was carried out by me under the supervision of Professor D. A. Tantrigoda and Dr. M. M. P. M. Fernando, and a report on this has not been submitted in whole or in part to any University or any other institution for another Degree/Diploma”.



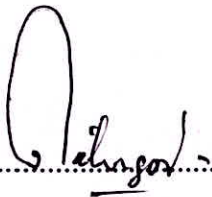
.....

Signature of the candidate

18.09.2013

Date

“We certify that the above statement made by the candidate is true and that this thesis is suitable for submission to the University for the purpose of evaluation”.



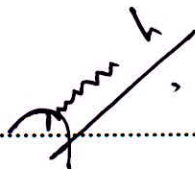
.....

Signature of the Supervisor

(Prof. D.A. Tantrigoda)

18.09.2013

Date



.....

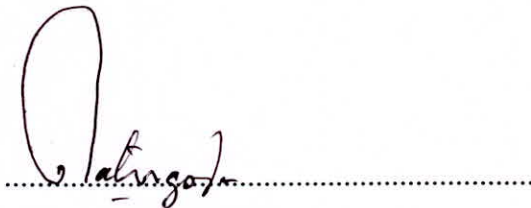
Signature of the Supervisor

(Dr. M.M.P.M. Fernando)

18.09.2013

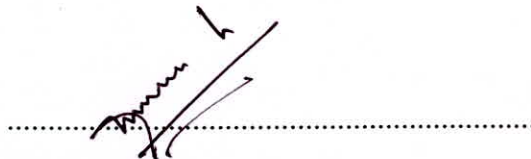
Date

“We certify that the candidate has incorporated all corrections, additions and amendments recommended by the examiners”.

A handwritten signature in black ink, appearing to read "D.A. Tantrigoda", written over a horizontal dotted line.

Signature of the Supervisor

(Prof. D.A. Tantrigoda)

A handwritten signature in black ink, appearing to read "Dr. M.M.P.M. Fernando", written over a horizontal dotted line.

Signature of the Supervisor

(Dr. M.M.P.M. Fernando)

Table of Contents

Table of contents	i
ABSTRACT	iv
ACKNOWLEDGEMENTS	vi
List of Figures.....	vii
List of Tables.....	xiii
List of Appendices.....	xiii
CHAPTER 01	1
INTRODUCTION	1
1.1 Introduction.....	1
1.2 Figure of the Earth and Gravity Anomalies.....	4
1.3 Magnetic Field of the Earth and Magnetic Anomalies	7
1.4 Objectives of the Study.....	9
1.5 An Over View Thesis	10
CHAPTER 02	12
METHODOLOGY	12
2.1 Interpretation of gravity anomalies	12
2.1.1 The Two-dimensional Interpretation Method	12
2.1.2 The end-correction Method.....	15
2.1.3 The Three-dimensional Interpretation Method	16
2.2 Interpretation of magnetic anomalies	20
2.2.1 Method of Interpretation	21
2.3 Validation of the Software	25
2.3.1 Validation of Software Developed for Two-dimensional Interpretation of Gravity Anomalies	25

2.3.2 Validation of the software for end-correction Method	32
2.3.3 Validation of the software for Three-dimensional Interpretation Method of Gravity Anomalies	34
2.3.4 Validation of the Software for the Interpretation Method of Magnetic Anomalies	38
CHAPTER 03	44
TWO AND THREE-DIMENSIONAL GRAVITY MODELS FOR THE SEDIMENTARY COVER OF SOUTHERN CONTINENTAL SHELF OF SRI LANKA	
3.1 Introduction.....	44
3.2 Two-Dimensional Interpretation.....	45
3.2.1 Two-Dimensional Interpretation of satellite gravity anomalies.....	45
3.2.2 Two-Dimensional Interpretation of ship-borne gravity anomalies	54
3.3 Three-Dimensional Interpretation of Satellite Gravity Anomalies.....	66
3.3.1 Interpretation of gravity anomalies over Block 01	66
3.3.2 Interpretation of gravity anomalies over Block 02	73
3.3.3 Interpretation of gravity anomalies over Block 03	78
CHAPTER 04	84
TWO DIMENSIONAL MAGNETIC MODEL FOR THE BASEMENT OF SEDIMENTARY COVER OF THE SOUTHERN OFF SHORE REGION OF SRI LANKA	
4.1 Introduction.....	84
4.2 Modeling of Magnetic Anomalies over the Southern off Shore Region of Sri Lanka	85
4.3 Comparison of magnetic results and gravity results	96
CHAPTER 5	102
CONCLUSIONS AND DISCUSSION.....	
5.1 Introduction.....	102

5.2 Discussion and Conclusions	102
5.3 Discussion and Suggestion for Future Work	105
REFERENCES	107
APPENDICES	110

8310 km², 6660 km² and 5263 km² with a maximum thickness of 3.3 km, 4.2 km and 4.2 km respectively. Further, average thickness and total sediment volume of sedimentary basins are 2.95 km, 3.73 km & 3.80 km and 14986 km³, 14103 km³ & 13678 km³ respectively.

Two dimensional and two and half dimensional interpretation of gravity anomalies and two dimensional interpretation of magnetic anomalies have been carried out using the conventional trial and error method. Interpretation of satellite gravity anomalies in three dimension has been carried using an iterative technique. Development of software needed for gravity and magnetic anomalies is an important part of the study in view of the very high cost of commercially available geophysical software. All the software used in the interpretation of gravity anomalies in two and three dimension have been developed as an integral part of the study using the Mathematica computer algebra package.

ACKNOWLEDGEMENTS

I would like to express my sincere appreciation to my principal supervisor Prof. D.A. Tantrigoda, Chair and Senior Professor of Physics, University of Sri Jayewardenepura for his constant guidance and encouragement, without which this work would not have been possible. I am truly grateful for his unwavering support. I am also grateful to my co-supervisor Dr. M. M. P. M. Fernando for his support towards the successful completion of my research work.

I am grateful to Dr. P. Geekiyanage for allowing me to carry out the study at the Department of Physics of University of Sri Jayewardenepura and providing me with necessary facilities.

I do extend my sincere appreciation to the Cairn Lankan Private Limited for kindly awarding me the financial support for this study. I would also like to thank Mr. Saliya Wickramasooriya and Mrs. Preeni Withanage, Director General and Director-Benefits, Petroleum Resources Development Secretariat, for providing me with ship borne gravity and magnetic data and for the support gave in many other ways.

List of Figures

Figure 1.1 Satellite free-air gravity anomaly contour map over the region 780E – 830E, 100N – 50N. Contour values are given in mGals. Three blocks subjected to the study are shown in the map.....	4
Figure 1.2 Reference ellipsoid of the Earth and equivalent sphere.....	6
Figure 2.1 Calculation of gravity anomaly at the origin due to a semi-infinite slab.....	14
Figure 2.2 Calculation of gravity anomaly at the origin due to a 2D body with a polygonal cross-section.....	14
Figure 2.3 Calculation of end correction factor. A is the perpendicular distance to the axis from the origin. y_1 and y_2 are the partial strike widths of the prism.....	16
Figure 2.4 Calculation of gravity anomaly at the plane of observation due to vertical elemental prisms. Reference plane, which delimits the top of the prism elements, is also shown.....	20
Figure 2.5 Calculation of magnetic anomaly at the origin due to a semi-infinite slab...	23
Figure 2.6 Alignment of magnetization vector J. A is the inclination of J, and B is the angle between its horizontal projection and the geographical North.....	23
Figure 2.7 Calculation of magnetic anomaly at the origin due to a 2D body with a polygonal cross-section.....	24
Figure 2.8 Gravity anomaly due to a causative body of density contrast (a) 0.3 g cm^{-3} and (b) 0.2 g cm^{-3}	26
Figure 2.9 Gravity anomaly due to a causative body of depth (a) 1 km and (b) 2 km..	27
Figure 2.10 Gravity anomaly due to a (a) symmetric causative body and (b) asymmetric causative body.....	27
Figure 2.11 Gravity anomaly caused by a (a) non-perturbed body and (b) perturbed body.....	28
Figure 2.12 Calculating the vertical component of gravity anomaly at a point P, due to an infinitely long horizontal cylinder of radius R, by using the direct method.....	29
Figure 2.13 Comparison of gravity anomalies calculated by using the direct method and polygonal method. (a) Blue color curve represents the anomaly calculated by using direct method and the red color curve represents the anomaly calculated by using polygonal method. (b) Infinitely long horizontal cylinder is shown by blue color and approximated polygonal body is shown by red color.....	31

Figure 2.14 Comparison of gravity anomalies due to a causative body, with and without introducing end corrections. (a) Blue color curve represents the anomaly calculated without introducing end corrections and red color curve represents the anomaly calculated by considering the end effects. (b) The causative body, which was divided into small horizontal prisms. Partial strike widths along the both directions of each prism are indicated on them.....	33
Figure 2.15 Calculating the vertical component of gravity anomaly at a point P on a grid, due to a sphere of radius R, by using the direct method.....	34
Figure 2.16 Contour map of gravity anomaly, which is to be utilized as the observed anomaly. This map was compiled by using gravity anomalies calculated by using the direct method. Gravity anomaly values are indicated on each contour line.....	35
Figure 2.17 (a) Contour map, compiled by using gravity anomalies caused by the derived model. Gravity anomaly values are indicated on each contour line. (b) A cross-section through the center of the derived model.....	36
Figure 2.18 (a) Comparison of observed gravity anomaly and calculated gravity anomaly due to the derived model along with a selected profile. (b). Comparison of cross sections of derived model and the original body. Gravity profiles and cross sections are selected across the center of the bodies.....	37
Figure 2.19 Magnetic anomalies caused by a body for different lengths of it.....	39
Figure 2.20 Magnetic anomalies caused by a body for different depths of it.....	40
Figure 2.21 Magnetic anomalies caused by a body for different angles of declination of the Earth's magnetic field.....	41
Figure 2.22 Magnetic anomalies caused by a body for different angles of inclination of the Earth's magnetic field.....	42
Figure 2.23 Magnetic anomalies caused by a body for different angles of inclination of the magnetization vector.....	43
Figure 3.1 Satellite bathymetry contour map over the region $78^{\circ}\text{E} - 83^{\circ}\text{E}$, $10^{\circ}\text{N} - 5^{\circ}\text{N}$. Contour values are given in meters.....	46
Figure 3.2 Five satellite gravity anomaly profiles, which were selected for the two dimensional interpretation. Thick straight lines represent the positions of the satellite gravity profiles and they were labeled as P1, P2, P3, P4 and P5.....	47
Figure 3.3 Interpretation of satellite gravity profile P1 of Figure 3.2. (a). Comparison of observed and calculated gravity anomalies. (b). Derived shallow structure below the gravity profile P1.....	49
Figure 3.4 Interpretation of satellite gravity profile P2 of Figure 3.2. (a). Comparison of observed and calculated gravity anomalies. (b). Derived shallow structure below the gravity profile P2.....	50

Figure 3.5 Interpretation of satellite gravity profile P3 of Figure 3.2. (a). Comparison of observed and calculated gravity anomalies. (b). Derived shallow structure below the gravity profile P3.....	51
Figure 3.6 Interpretation of satellite gravity profile P4 of Figure 3.2. (a). Comparison of observed and calculated gravity anomalies. (b). Derived shallow structure below the gravity profile P4.....	52
Figure 3.7 Interpretation of satellite gravity profile P5 of Figure 3.2. (a). Comparison of observed and calculated gravity anomalies. (b). Derived shallow structure below the gravity profile P5.....	53
Figure 3.8 Positions of the ship-born gravity anomaly profiles, which were subjected to the two dimensional interpretation. They were labeled from P1 to P9.....	55
Figure 3.9 Interpretation of ship-born gravity profile P1 of Figure 3.8. (a). Comparison of observed and calculated gravity anomalies. (b). Derived shallow structure below the gravity profile P1.....	57
Figure 3.10 Interpretation of ship-born gravity profile P2 of Figure 3.8. (a). Comparison of observed and calculated gravity anomalies. (b). Derived shallow structure below the gravity profile P2.....	58
Figure 3.11 Interpretation of ship-born gravity profile P3 of Figure 3.8. (a). Comparison of observed and calculated gravity anomalies. (b). Derived shallow structure below the gravity profile P3.....	59
Figure 3.12 Interpretation of ship-born gravity profile P4 of Figure 3.8. (a). Comparison of observed and calculated gravity anomalies. (b). Derived shallow structure below the gravity profile P4.....	60
Figure 3.13 Interpretation of ship-born gravity profile P5 of Figure 3.8. (a). Comparison of observed and calculated gravity anomalies. (b). Derived shallow structure below the gravity profile P5.....	61
Figure 3.14 Interpretation of ship-born gravity profile P6 of Figure 3.8. (a). Comparison of observed and calculated gravity anomalies. (b). Derived shallow structure below the gravity profile P6.....	62
Figure 3.15 Interpretation of ship-born gravity profile P7 of Figure 3.8. (a). Comparison of observed and calculated gravity anomalies. (b). Derived shallow structure below the gravity profile P7.....	63
Figure 3.16 Interpretation of ship-born gravity profile P8 of Figure 3.8. (a). Comparison of observed and calculated gravity anomalies. (b). Derived shallow structure below the gravity profile P8.....	64
Figure 3.17 Interpretation of ship-born gravity profile P9 of Figure 3.8. (a). Comparison of observed and calculated gravity anomalies. (b). Derived shallow structure below the gravity profile P9.....	65
Figure 3.18 Satellite gravity anomaly contour map over block 01 of the study region.....	67

Figure 3.19 Satellite bathymetry contour map over block 01 of the study region.....	68
Figure 3.20 Sediment thickness contour map of derived model corresponding to the block 01. Density of oceanic sediments has been assumed as 2300 kgm^{-3} in the interpretation. Positions of four selected sediment thickness profiles P1, P2, P3 and P4, are also shown.....	69
Figure 3.21 Sediment thickness contour map of derived model corresponding to the block 01. Density of oceanic sediments has been assumed as 2600 kgm^{-3} in the interpretation. Positions of four selected sediment thickness profiles P1, P2, P3 and P4, are also shown.....	70
Figure 3.22 Comparison of sediment thickness below the profile P1 obtained from two interpretations using densities 2300 kgm^{-3} and 2600 kgm^{-3} for oceanic sediment.....	71
Figure 3.23 Comparison of sediment thickness below the profile P2 obtained from two interpretations using densities 2300 kgm^{-3} and 2600 kgm^{-3} for oceanic sediment.....	71
Figure 3.24 Comparison of sediment thickness below the profile P3 obtained from two interpretations using densities 2300 kgm^{-3} and 2600 kgm^{-3} for oceanic sediment.....	72
Figure 3.25 Comparison of sediment thickness below the profile P4 obtained from two interpretations using densities 2300 kgm^{-3} and 2600 kgm^{-3} for oceanic sediment.	72
Figure 3.26 Satellite gravity anomaly contour map over block 02 of the study region.	74
Figure 3.27 Satellite bathymetry contour map over block 02 of the study region.....	74
Figure 3.28 Sediment thickness contour map of derived model corresponding to the block 02. Density of oceanic sediments has been assumed as 2300 kgm^{-3} in the interpretation. Positions of four selected sediment thickness profiles P5, P6, P7 and P8, are also shown.....	75
Figure 3.29 Sediment thickness contour map of derived model corresponding to the block 02. Density of oceanic sediments has been assumed as 2600 kgm^{-3} in the interpretation. Positions of four selected sediment thickness profiles P5, P6, P7 and P8, are also shown.....	75
Figure 3.30 Comparison of sediment thickness below the profile P5 obtained from two interpretations using densities 2300 kgm^{-3} and 2600 kgm^{-3} for oceanic sediment.....	76
Figure 3.31 Comparison of sediment thickness below the profile P6 obtained from two interpretations using densities 2300 kgm^{-3} and 2600 kgm^{-3} for oceanic sediment.....	76
Figure 3.32 Comparison of sediment thickness below the profile P7 obtained from two interpretations using densities 2300 kgm^{-3} and 2600 kgm^{-3} for oceanic sediment.....	77
Figure 3.33 Comparison of sediment thickness below the profile P8 obtained from two interpretations using densities 2300 kgm^{-3} and 2600 kgm^{-3} for oceanic sediment.....	77
Figure 3.34 Satellite gravity anomaly contour map over block 03 of the study region.	79

Figure 3.35 Satellite bathymetry contour map over block 03 of the study region.....	79
Figure 3.36 Sediment thickness contour map of derived model corresponding to the block 03. Density of oceanic sediments has been assumed as 2300 kgm^{-3} in the interpretation. Positions of four selected sediment thickness profiles, P9, P10, P11 and P12, are also shown.....	80
Figure 3.37 Sediment thickness contour map of derived model corresponding to the block 03. Density of oceanic sediments has been assumed as 2600 kgm^{-3} in the interpretation. Positions of four selected sediment thickness profiles, P9, P10, P11 and P12, are also shown.....	81
Figure 3.38 Comparison of sediment thickness along profile P9 obtained from two interpretations using densities 2300 kgm^{-3} and 2600 kgm^{-3} for oceanic sediment.....	82
Figure 3.39 Comparison of sediment thickness along profile P10 obtained from two interpretations using densities 2300 kgm^{-3} and 2600 kgm^{-3} for oceanic sediment.....	82
Figure 3.40 Comparison of sediment thickness along profile P11 obtained from two interpretations using densities 2300 kgm^{-3} and 2600 kgm^{-3} for oceanic sediment.....	83
Figure 3.41 Comparison of sediment thickness along profile P12 obtained from two interpretations using densities 2300 kgm^{-3} and 2600 kgm^{-3} for oceanic sediment.....	83
Figure 4.1 Positions of the ship-born magnetic anomaly profiles, which were subjected to the two dimensional interpretation. They were labeled from P1 to P9.....	86
Figure 4.2 Interpretation of ship-born magnetic anomaly profile P1 of Figure 4.1. (a) Comparison of observed and calculated magnetic anomalies. (b) Derived shallow structure below the magnetic profile P1.....	87
Figure 4.3 Interpretation of ship-born magnetic anomaly profile P2 of Figure 4.1. (a) Comparison of observed and calculated magnetic anomalies. (b) Derived shallow structure below the magnetic profile P2.....	88
Figure 4.4 Interpretation of ship-born magnetic anomaly profile P3 of Figure 4.1. (a) Comparison of observed and calculated magnetic anomalies. (b) Derived shallow structure below the magnetic profile P3.....	89
Figure 4.5 Interpretation of ship-born magnetic anomaly profile P4 of Figure 4.1. (a) Comparison of observed and calculated magnetic anomalies. (b) Derived shallow structure below the magnetic profile P4.....	90
Figure 4.6 Interpretation of ship-born magnetic anomaly profile P5 of Figure 4.1. (a) Comparison of observed and calculated magnetic anomalies. (b) Derived shallow structure below the magnetic profile P5.....	91
Figure 4.7 Interpretation of ship-born magnetic anomaly profile P6 of Figure 4.1. (a) Comparison of observed and calculated magnetic anomalies. (b) Derived shallow structure below the magnetic profile P6.....	92

Figure 4.8 Interpretation of ship-born magnetic anomaly profile P7 of Figure 4.1. (a) Comparison of observed and calculated magnetic anomalies. (b) Derived shallow structure below the magnetic profile P7.....	93
Figure 4.9 Interpretation of ship-born magnetic anomaly profile P8 of Figure 4.1. (a) Comparison of observed and calculated magnetic anomalies. (b) Derived shallow structure below the magnetic profile P8.....	94
Figure 4.10 Interpretation of ship-born magnetic anomaly profile P9 of Figure 4.1. (a) Comparison of observed and calculated magnetic anomalies. (b) Derived shallow structure below the magnetic profile P9.....	95
Figure 4.11 Comparison of the depth to the basement of the sedimentary cover below the profile P1 obtained from gravity and magnetic modeling (Figure 3.9 and Figure 4.2). Depth to the basement of the sedimentary cover obtained from the joint gravity and magnetic studies is also shown.....	97
Figure 4.12 Comparison of the depth to the basement of the sedimentary cover below the profile P2 obtained from gravity and magnetic modeling (Figure 3.10 and Figure 4.3). Depth to the basement of the sedimentary cover obtained from the joint gravity and magnetic studies is also shown.....	98
Figure 4.13 Comparison of the depth to the basement of the sedimentary cover below the profile P3 obtained from gravity and magnetic modeling (Figure 3.11 and Figure 4.4). Depth to the basement of the sedimentary cover obtained from the joint gravity and magnetic studies is also shown.....	98
Figure 4.14 Comparison of the depth to the basement of the sedimentary cover below the profile P4 obtained from gravity and magnetic modeling (Figure 3.12 and Figure 4.5). Depth to the basement of the sedimentary cover obtained from the joint gravity and magnetic studies is also shown.....	99
Figure 4.15 Comparison of the depth to the basement of the sedimentary cover below the profile P5 obtained from gravity and magnetic modeling (Figure 3.13 and Figure 4.6). Depth to the basement of the sedimentary cover obtained from the joint gravity and magnetic studies is also shown.....	99
Figure 4.16 Comparison of the depth to the basement of the sedimentary cover below the profile P6 obtained from gravity and magnetic modeling (Figure 3.14 and Figure 4.7). Depth to the basement of the sedimentary cover obtained from the joint gravity and magnetic studies is also shown.....	100
Figure 4.17 Comparison of the depth to the basement of the sedimentary cover below the profile P7 obtained from gravity and magnetic modeling (Figure 3.15 and Figure 4.8). Depth to the basement of the sedimentary cover obtained from the joint gravity and magnetic studies is also shown.....	100
Figure 4.18 Comparison of the depth to the basement of the sedimentary cover below the profile P8 obtained from gravity and magnetic modeling (Figure 3.16 and Figure 4.9). Depth to the basement of the sedimentary cover obtained from the joint gravity and magnetic studies is also shown.....	101